Incorporating Non-Linear Tire Dynamics into a Convex Approach to Shared Steering Control

Stephen M. Erlien[1,2], Joseph Funke[1], and J. Christian Gerdes[1]

***Abstract*— Active safety systems enabled by steer-by-wire technology can share control with a driver, augmenting the driver's steering commands to avoid collisions and prevent loss of control. The extent to which this can be done is limited by the controller's ability to anticipate dangerous scenarios in order to appropriately intervene and steer the vehicle to safety. However, the non-linear nature of tire dynamics poses a challenge in predicting and modifying vehicle behavior in real-time. In this paper, online successive linearizations of the future planned vehicle trajectory approximates these non-linear dynamics in a real-time, model predictive controller that shares control with a human driver. Simulation results of aggressive maneuvers demonstrate the usefulness of this approach as well as illustrate interesting interactions between the sometimes competing objectives of vehicle stability and collision avoidance.**

I. INTRODUCTION

Steer-by-wire is a technology that eliminates the mechanical connection between the driver's hand wheel and the front road wheels. This enables active safety systems to have significant control over the lateral dynamics of the vehicle through augmentation of the driver's steering command. In addition, Hsu et al. [1] demonstrated that steer-by-wire enables real-time road surface friction and vehicle state estimation. With these enhanced actuation and sensing capabilities, combined with advances in perception technologies, active safety systems have the potential to avoid collisions in addition to providing vehicle stability.

Model Predictive Control (MPC) is a useful framework for leveraging these new capabilities [2][3]. MPC schemes fall into two general categories: those that leverage convex optimization and those that do not. The latter benefits from direct consideration of non-linear models in the optimization at the expense of run-time performance and solver reliability. The former benefits from efficient, reliable solvers for fast implementation at the expense of being restricted to affine models. However, use of online successive linearizations enables convex MPC schemes to approximate non-linear plant dynamics. In these schemes, the controller optimizes the plant's trajectory using a linear time-varying plant model derived from the optimized trajectory from the controller's previous execution. Falcone et al. [3] use this technique in a real-time path tracking controller intended for a fully autonomous system. Timing and Cole [4] use successive linearizations as an efficient alternative to non-linear optimization in an off-line algorithm for generating racing lines. In this paper, the successive linearizations technique is applied to a real-time controller that shares control with a human driver using safe driving envelopes. This enables the controller to anticipate challenges in maintaining vehicle stability and collision avoidance at the limits of handling without restricting the driver to a predefined path.

The safe envelopes used in this work were previously presented by the authors as a driver assistance framework for obstacle avoidance and stability control [5]. One of these envelopes enforces vehicle stability while the other ensures collision free trajectories. With only the ability to steer, situations may arise in which adherence to both envelopes is not possible. In this work, a MPC scheme uses successive linearizations to model the effects of tire saturation in predicting future vehicle behavior relative to these two envelopes. Simulation results demonstrate this enables more accurate prediction of situations in which vehicle stability needs to be sacrificed in order to ensure collision avoidance. The paper concludes with a discussion of how this work informs future envelope control development.

II. VEHICLE MODEL

The vehicle model used in the online MPC controller is a constant speed, planar bicycle model with five states. The vehicle's motion is described by two of the states: sideslip β and yaw rate r. These are defined in Figure 1 and have the following equations of motion:

$$\dot{\beta} = \frac{F_{\mathrm{yf}} + F_{\mathrm{yr}}}{mU_{\mathrm{x}}} - r \qquad \dot{r} = \frac{aF_{\mathrm{yf}} - bF_{\mathrm{yr}}}{I_{\mathrm{zz}}} \tag{1}$$

where $F_{\mathrm{y[f,r]}}$ is the lateral tire force of the [front, rear] axle, m is the vehicle mass, U_{x} is the longitudinal velocity in the body fixed frame, I_{zz} is the yaw inertia, and a and b are the distances from the center of gravity to the front and rear

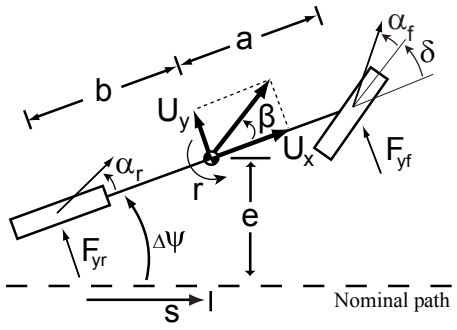

Fig. 1. Bicycle model schematic

[1]Department of Mechanical Engineering at Stanford University, Stanford, California, USA.

[2]This is the corresponding author. serlien@stanford.edu

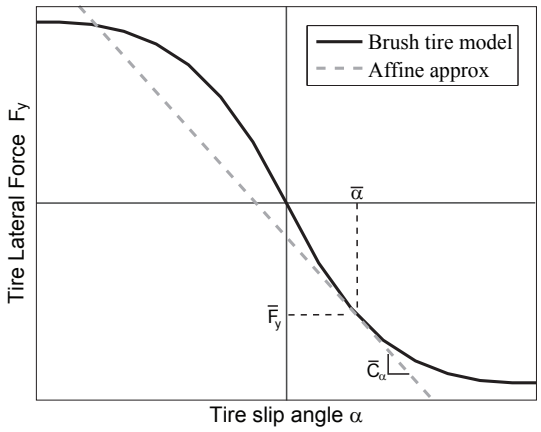

Fig. 2. Brush tire model with affine approximation at $\bar{\alpha}$

axles, respectively. The tire slip angles, α_{f} and α_{r}, can be expressed as:

$$\alpha_{\mathrm{f}} = \tan^{-1}\left(\beta + \frac{ar}{U_{\mathrm{x}}}\right) - \delta \approx \beta + \frac{ar}{U_{\mathrm{x}}} - \delta \quad (2)$$

$$\alpha_{\mathrm{r}} = \tan^{-1}\left(\beta - \frac{br}{U_{\mathrm{x}}}\right) \approx \beta - \frac{br}{U_{\mathrm{x}}} \quad (3)$$

where δ is the front steer angle, and small angle approximations give linear expressions. The brush tire model proposed by Fiala [6] and presented in the following form by Pacejka [7] describes the relationship between $F_{\mathrm{y[f,r]}}$ and $\alpha_{\mathrm{[f,r]}}$:

$$F_{\mathrm{y}} = \begin{cases} -C_\alpha \tan\alpha + \frac{C_\alpha^2}{3\mu F_{\mathrm{z}}}|\tan\alpha|\tan\alpha \ldots \\ \qquad -\frac{C_\alpha^3}{27\mu^2 F_{\mathrm{z}}^2}\tan^3\alpha, \quad |\alpha| < \tan^{-1}\left(\frac{3\mu F_{\mathrm{z}}}{C_\alpha}\right) \\ -\mu F_{\mathrm{z}} \mathrm{sgn}\ \alpha, \qquad \text{otherwise} \end{cases} \quad (4)$$

$$= f_{\mathrm{tire}}(\alpha) \quad (5)$$

where μ is the surface coefficient of friction, F_{z} is the normal load, and C_α is the tire cornering stiffness.

The input to the vehicle model is F_{yf}, which is mapped to δ using (2) and (5):

$$\delta = \beta + \frac{ar}{U_{\mathrm{x}}} - f_{\mathrm{tire}}^{-1}(F_{\mathrm{yf}}) \quad (6)$$

where f_{tire}^{-1} is computed numerically and real-time estimates of β and r are assumed to be available.

Use of F_{yf} as the model input enables explicit consideration of the non-linear dynamics of the front tires. However, this approach does not work for modeling rear tire dynamics unless the vehicle is equipped with rear steering actuation. Instead, a linearization of the brush tire model at a given rear tire slip angle, $\bar{\alpha}_{\mathrm{r}}$, models rear tire force, F_{yr}, as an affine function of α_{r}:

$$F_{\mathrm{yr}} = \bar{F}_{\mathrm{yr}} - \bar{C}_{\bar{\alpha}_{\mathrm{r}}}(\alpha_{\mathrm{r}} - \bar{\alpha}_{\mathrm{r}}) \quad (7)$$

where $\bar{F}_{\mathrm{yr}} = f_{\mathrm{tire}}(\bar{\alpha}_{\mathrm{r}})$ and $\bar{C}_{\bar{\alpha}_{\mathrm{r}}}$ is the equivalent cornering stiffness at $\bar{\alpha}_{\mathrm{r}}$. This is illustrated in Figure 2.

In the near term of the prediction horizon, this rear tire model is linearized around the measured rear tire slip angle, α_{r}, as was done by Beal and Gerdes [8]. Over this short horizon, the vehicle states do not change significantly, which enables accurate prediction of vehicle state propagation in the near term.

The appropriate choice of $\bar{\alpha}_{\mathrm{r}}$ in the remainder of the prediction horizon is the main topic of this paper. Two possibilities will be evaluated and compared. The first is naively choosing $\bar{\alpha}_{\mathrm{r}}^{(k)} = 0$, which results in a linear tire model for time steps k in the latter portion of the horizon as was used in previous work [5]. The second approach is to choose $\bar{\alpha}_{\mathrm{r}}^{(k)} = \hat{\alpha}_{\mathrm{r}}^{(k)}$, where $\hat{\alpha}_{\mathrm{r}}^{(k)}$ is the predicted rear slip angle at time step k from the optimal trajectory computed in the previous controller execution. This use of successive linearizations provides an approximation to the non-linear tire behavior throughout the entire prediction horizon.

For both of these approaches, the equations of motion can be expressed as affine functions of the states and input:

$$\dot{\beta} = \frac{F_{\mathrm{yf}} + \bar{F}_{\mathrm{yr}} - \bar{C}_{\bar{\alpha}_{\mathrm{r}}}\left(\beta - \frac{br}{U_{\mathrm{x}}} - \bar{\alpha}_{\mathrm{r}}\right)}{mU_{\mathrm{x}}} - r \quad (8)$$

$$\dot{r} = \frac{aF_{\mathrm{yf}} - b\left[\bar{F}_{\mathrm{yr}} - \bar{C}_{\bar{\alpha}_{\mathrm{r}}}\left(\beta - \frac{br}{U_{\mathrm{x}}} - \bar{\alpha}_{\mathrm{r}}\right)\right]}{I_{zz}} \quad (9)$$

The position of the vehicle relative to a nominal path is given by the remaining three states: heading deviation $\Delta\psi$, lateral deviation e, and distance along the path s as defined in Figure 1.

The equations of motion of these states can be written as:

$$\dot{\Delta\psi} = r \quad (10)$$

$$\dot{e} = U_{\mathrm{x}}\sin(\Delta\psi) + U_{\mathrm{y}}\cos(\Delta\psi) \quad (11)$$

$$\approx U_{\mathrm{x}}\Delta\psi + U_{\mathrm{x}}\beta \quad (12)$$

$$\dot{s} = U_{\mathrm{x}}\cos(\Delta\psi) - U_{\mathrm{y}}\sin(\Delta\psi) \quad (13)$$

$$\approx U_{\mathrm{x}} - U_{\mathrm{x}}\beta\Delta\psi \approx U_{\mathrm{x}} \quad (14)$$

where small angle assumptions for $\Delta\psi$ and β give the simplified expressions.

Combining (8), (9), (10), (12), and (14), a discrete, time-varying vehicle model is expressed as:

$$x^{(k+1)} = A_{\bar{\alpha}_{\mathrm{r}},t_{\mathrm{s}}}^{(k)} x^{(k)} + B_{\bar{\alpha}_{\mathrm{r}},t_{\mathrm{s}}}^{(k)} {F_{\mathrm{yf}}}^{(k)} + d_{\bar{\alpha}_r,t_s}^{(k)} \quad (15)$$

where $x = [\beta \quad r \quad \Delta\psi \quad s \quad e]^T$, k is a time step index, subscript $\bar{\alpha}_{\mathrm{r}}$ denotes linearization of the rear tire model around rear slip angle $\bar{\alpha}_{\mathrm{r}}$, and subscript t_{s} denotes discretization of the vehicle model using time step length t_{s}.

III. Safe Driving Envelopes

The safe driving envelopes used in this work were previously presented by the authors [5] and summarized here.

A. Stable Handling Envelope

Originally presented by Beal and Gerdes, the stable handling envelope defines limits on the states describing the vehicle's motion as illustrated in Figure 3. This envelope reflects the maximum capabilities of the vehicle's tires so at any point within this envelope, there exists a steering command to safely remain inside, ensuring stability [8].

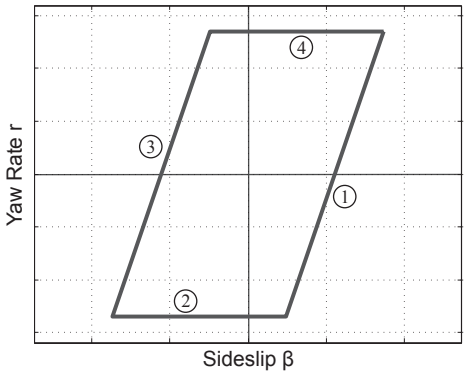

Fig. 3. Stable handling envelope

The maximum steady-state yaw rate defines bounds (2) and (4) in Figure 3. Neglecting the effects of weight transfer and assuming zero longitudinal tire forces, the steady-state condition of (1) gives an expression for the maximum steady-state yaw rate:

$$r_{\mathrm{ss,max}} = \frac{F_{\mathrm{yf,max}} + F_{\mathrm{yr,max}}}{mU_{\mathrm{x}}} = \frac{g\mu}{U_{\mathrm{x}}} \tag{16}$$

where g is the gravitational constant.

Another important consideration for vehicle stability is the saturation of the rear tires [8][9]. The final two bounds of the vehicle envelope serve to limit the rear slip angle to the angle at which lateral force saturates. For brush tire model (4), this is expressed as:

$$\alpha_{\mathrm{r,sat}} = \tan^{-1}\left(3\frac{mg\mu}{C_{\alpha_{\mathrm{r}}}}\frac{a}{a+b}\right) \tag{17}$$

With this bound on rear slip angle, the maximum sideslip, which serves as the basis for bounds (1) and (3) in Figure 3, can be determined from (3):

$$\beta_{\max} = \alpha_{\mathrm{r,sat}} + \frac{br}{U_{\mathrm{x}}} \tag{18}$$

The desire to restrain the vehicle states within the stable handling envelope, whose bounds are defined by (16) and (18), will be compactly expressed as the inequality:

$$\left|H_{\mathrm{sh}}x^{(k)}\right| \leq G_{\mathrm{sh}} \tag{19}$$

where subscript sh indicates the stable handling envelope.

B. Environmental Envelope

The environmental envelope consists of a set of collision free tubes along the nominal path like the two illustrated in Figure 4. To avoid collision with the environment, the vehicle's trajectory must be fully contained within any one of these tubes. Each tube defines time-varying constraints on the lateral deviation of the vehicle from the nominal path:

$$e^{(k)} \leq e^{(k)}_{\max} - \frac{1}{2}d - d_{\mathrm{buffer}} \tag{20}$$

$$e^{(k)} \geq e^{(k)}_{\min} + \frac{1}{2}d + d_{\mathrm{buffer}} \tag{21}$$

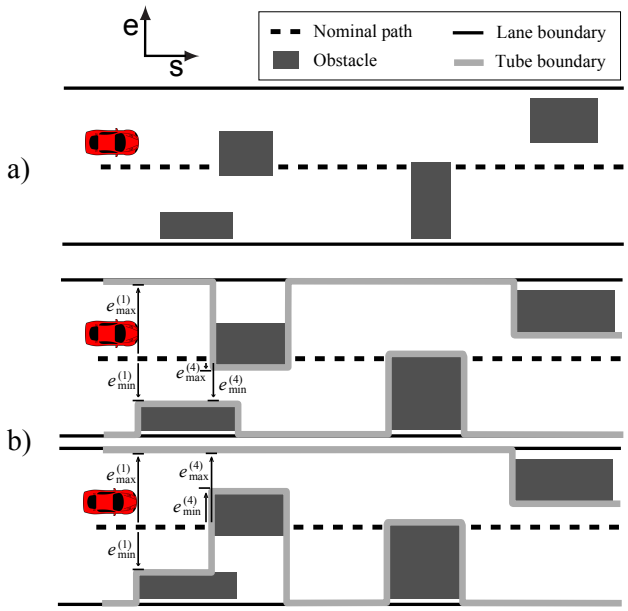

Fig. 4. The environmental envelope is a representation of a) a collection of obstacles along the nominal path using b) tubes (two of them in this example) which define a maximum ($e^{(k)}_{\max}$) and minimum ($e^{(k)}_{\min}$) lateral deviation from the nominal path at each time step, k.

where $e^{(k)}_{\max}$ and $e^{(k)}_{\min}$ indicate the lateral deviation bounds for time step k, d is the vehicle's width, and d_{buffer} specifies a preferred minimum distance between obstacles and the vehicle to ensure driver comfort.

For any two trajectories generated using vehicle model (15) and contained within a tube, the linear combination of those trajectories will also be contained within that same tube. Therefore, the set of collision free trajectories corresponding to a single tube is a convex set, which enables the use of fast optimization techniques to quickly identify optimal trajectories.

Inequalities (20) and (21) will be compactly expressed as:

$$H_{\mathrm{env}}x^{(k)} \leq G^{(k)}_{\mathrm{env}} \tag{22}$$

where subscript env indicates the environmental envelope.

A vehicle trajectory is collision free throughout the prediction horizon if and only if it satisfies inequality (22) for all k for any *one* tube in the environmental envelope. In this paper, the environments that are considered can all be represented using only one tube; however, a discussion of how to handle multi-tube environments along with the methodology to generate these tubes in real-time has been previously published [5].

IV. MPC Formulation

The controller's primary task is to ensure safe vehicle operation within the previously defined safe driving envelopes. Additionally, it should be minimally invasive to the driver while avoiding harsh interventions. The first of these additional objectives is modeled as identically matching the driver's present steering command. The latter of these

additional objectives is modeled as a preference for future trajectories with smooth steering commands. The overall objectives of the controller can be expressed as an optimal control problem to be evaluated over a finite prediction horizon:

$$\begin{aligned}
\text{minimize} \quad & \left| F_{\text{yf,driver}} - F^{(0)}_{\text{yf,opt}} \right| && \text{(23a)}\\
& + \sum_k \gamma^{(k)} \left|\left| F^{(k)}_{\text{yf,opt}} - F^{(k-1)}_{\text{yf,opt}} \right|\right|_2 && \text{(23b)}\\
& + \sum_k \begin{bmatrix} \sigma_{\text{sh}} & \sigma_{\text{sh}} \end{bmatrix} S^{(k)}_{\text{sh,opt}} && \text{(23c)}\\
& + \sum_k \begin{bmatrix} \sigma_{\text{env}} & \sigma_{\text{env}} \end{bmatrix} S^{(k)}_{\text{env,opt}} && \text{(23d)}\\
\text{subject to} \quad & x^{(k+1)} = A^{(k)}_{\bar{\alpha}_{\text{r}},t_{\text{s}}} x^{(k)} + B^{(k)}_{\bar{\alpha}_{\text{r}},t_{\text{s}}} F^{(k)}_{\text{yf,opt}} + d^{(k)}_{\bar{\alpha}_{\text{r}},t_{\text{s}}} && \text{(23e)}\\
& \left| F^{(k)}_{\text{yf,opt}} \right| \leq F_{\text{yf,max}} && \text{(23f)}\\
& \left| H_{\text{sh}} x^{(k+1)} \right| \leq G_{\text{sh}} + S^{(k)}_{\text{sh,opt}} && \text{(23g)}\\
& H_{\text{env}} x^{(k+1)} \leq G^{(k+1)}_{\text{env}} + S^{(k)}_{\text{env,opt}} && \text{(23h)}\\
& \left| F^{(k)}_{\text{yf,opt}} - F^{(k-1)}_{\text{yf,opt}} \right| \leq F^{(k)}_{\text{yf,max slew}} && \text{(23i)}\\
& k = 0 \ldots 29
\end{aligned}$$

where the variables to be optimized are the optimal input trajectory ($F_{\text{yf,opt}}$) and the safe driving envelope slack variables ($S_{\text{sh,opt}}$, $S_{\text{env,opt}}$). As is commonly done in MPC, only the optimal input for the first step into the prediction horizon, $F^{(0)}_{\text{yf,opt}}$, is applied to the vehicle, and optimization problem (23) is re-solved at the next time step.

Tunable parameters in this optimization are the slack variable costs (σ_{sh}, σ_{env}) and γ, which establishes the trade-off between a smooth input trajectory (23b) and matching the driver's present steering command (23a). Cost term (23a) uses the l_1 norm as a convex approximation to the objective of *identically matching* the driver's command where $F_{\text{yf,driver}}$ is the front tire force corresponding to the driver's steering wheel command, δ_{driver}. Brush tire model (5) provides the mapping from δ_{driver} to $F_{\text{yf,driver}}$:

$$F_{\text{yf,driver}} \quad = \quad f_{\text{tire}} \left(\beta + \frac{ar}{U_x} - \delta_{\text{driver}} \right) \qquad (24)$$

Constraint (23f) reflects the maximum force capabilities of the front tires and (23i) reflects the slew rate limit of the vehicle steering system. Constraints (23g) and (23h) enforce the stable handling and environmental envelopes, respectively. These constraints are softened with slack variables, $S_{\text{sh,opt}}$ and $S_{\text{env,opt}}$, to ensure optimization (23) is always feasible. With the choice of sufficiently large σ_{sh} and σ_{env}, cost terms (23c) and (23d) encourage zero-valued slack variables, resulting in optimal vehicle trajectories that adhere to both safe driving envelopes whenever possible. In addition, the slack variable costs are chosen such that $\sigma_{\text{env}} >> \sigma_{\text{sh}}$, which establishes a hierarchy between the two safe driving envelopes, prioritizing collision avoidance over vehicle stability. This trade-off will be explored in the simulations that follow.

TABLE I

PREDICTION HORIZON PARAMETERS

Parameter	**Near Term Horizon**	**Long Term Horizon**
k	0...9	10...29
$t_{\text{s}}^{(k)}$	0.01 [s]	0.2 [s]
$\gamma^{(k)}$	30	1.5
$F^{(k)}_{\text{yf,max slew}}$	0.2 [kN]	5 [kN]
σ_{sh}	60	60
σ_{env}	1500	1500
$\bar{\alpha}_{\text{r}}^{(k)}$	α_{r}	0 (Linear Model) or $\hat{\alpha}_{\text{r}}^{(k)}$ (Approx Non-Linear Model)

The prediction horizon used in optimization (23) uses different length time steps in the near and long terms of the horizon to consider obstacles in the long term without compromising the prediction of vehicle states in the near term. Table I gives the values of parameters in these two portions of the prediction horizon.

CVXGEN [10] is used to leverage the significantly sparse structure of convex optimization problem (23) to produce an efficient solver for real-time implementation [11].

V. SIMULATION RESULTS

Simulations of the controller using both approaches to rear tire modeling demonstrate the value of approximating non-linear rear tire behavior using successive linearizations over the simpler linear rear tire model. Table II lists the parameters of the vehicle used in the following simulations, which represent Stanford's P1 steer-by-wire research testbed. In these simulations, the arrangement of obstacles, as illustrated in Figure 5, requires the vehicle to execute a double lane change to avoid a collision. For simplicity, the effects of vehicle roll and weight transfer are ignored in the following simulations.

TABLE II

VEHICLE PARAMETERS

Parameter	Value	Units
m	1725	kg
I_z	1300	$\text{kg} \cdot \text{m}^2$
a	1.35	m
b	1.15	m
d	1.60	m
$\text{C}_{\alpha f}$	57.8	$\text{kN} \cdot \text{rad}^{-1}$
$\text{C}_{\alpha r}$	110	$\text{kN} \cdot \text{rad}^{-1}$

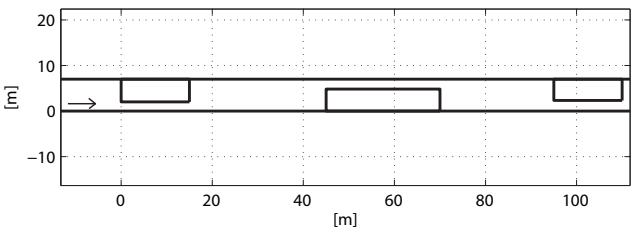

Fig. 5. Arrangement of obstacles and road boundaries used in the following simulations. Vehicle travels in the direction indicated by the arrow.

Figure 6 illustrates the shared control capabilities of the controller at a moderate speed of 12 [m/s] on a low friction surface ($\mu = 0.55$). Using either tire model, the controller successfully augments the human driver's steering command to negotiate the double lane change. The driver is modeled using an open-loop steering command which, at this speed, almost navigates the obstacles without collision or loss of control. However, as illustrated, two slight augmentations of the driver's command are required to avoid collision, and the controller identically matches the driver's command otherwise.

Figure 7 provides a comparison of the controller's performance at a more aggressive speed of 16 [m/s] on the same low friction surface. At this speed, the controller fails to avoid collision with the road boundary without considering rear tire saturation in the latter portion of the prediction horizon. Recall that both versions of the controller consider rear tire saturation in the near term of the horizon; however, only when the controller considers this saturation throughout the entire horizon is it able to successfully avoid violation of either safe driving envelope with only moderate augmentation of the driver's command.

With only the ability to steer, situations arise when adherence to both safe driving envelopes is impossible, as illustrated in Figure 8 where the speed is 18 [m/s]. The combination of low friction and high speed forces the controller to violate one of the envelopes. According to the envelope hierarchy dictated by the relative weights discussed in Section IV, the controller prioritizes collision avoidance over vehicle stability as illustrated in the bottom plot of Figure 8. However, only when the controller considers future saturation of the rear tires is it able to safely augment the driver's command to avoid collision. Using the linear rear tire model, the controller is ultimately able to stabilize the vehicle only after allowing it to get significantly sideways and collide with the road boundary.

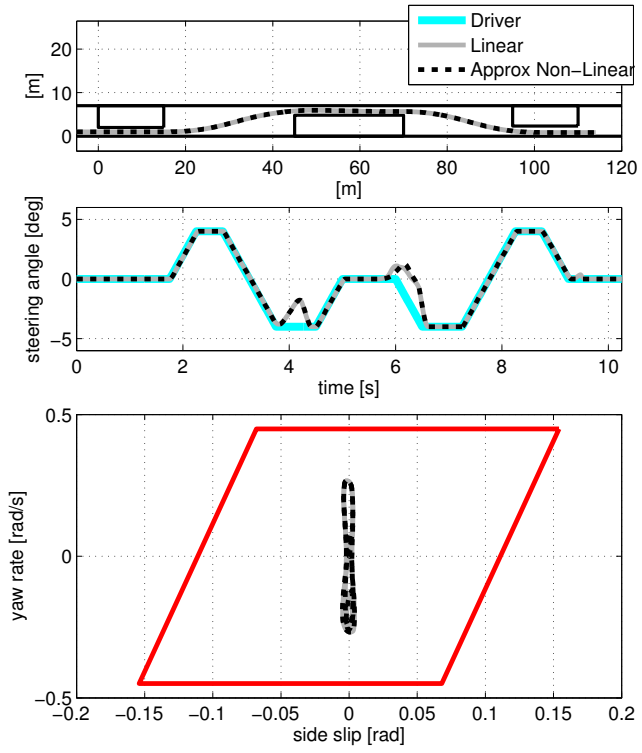

Fig. 6. Double lane change maneuver on low friction surface at 12 [m/s]

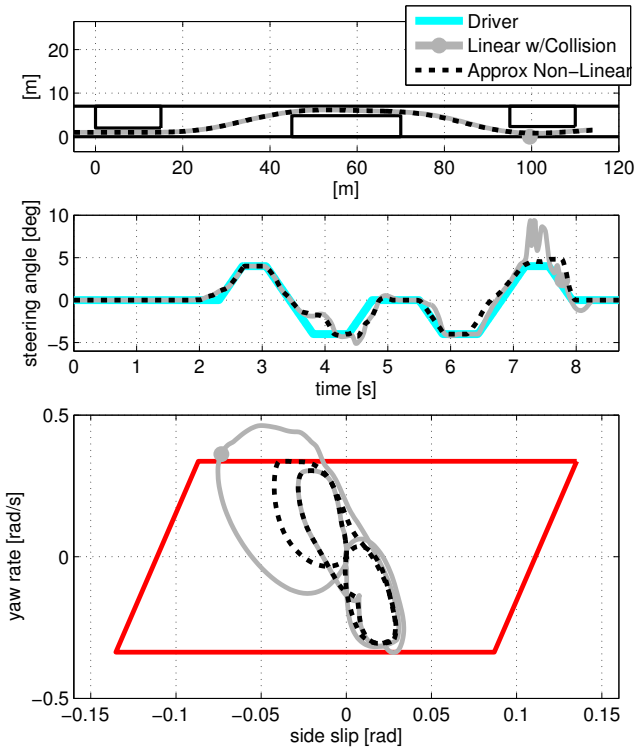

Fig. 7. Double lane change maneuver on low friction surface at 16 [m/s]

Figure 9 displays a comparison of the internal predictions by the controller of the future vehicle states using each of the rear tire models. As expected, in both cases the controller accurately predicts the pending stable handling envelope violation because the current rear slip angle is used to predict near term rear tire behavior in both cases. However, as illustrated on the left of Figure 9, use of a linear model in the remainder of the prediction horizon underestimates the extent of this envelope violation. This leads the controller to make steering decisions that result in significant violation of the safe handling envelope followed by a collision with the road boundary. The approximate non-linear rear tire model better predicts future vehicle states, and, as seen in the right of Figure 9, the controller plans a slight violation of the stable handling envelope in order to prevent significant violations in the future and avoid collision with the environment.

Additional simulations reveal a similar trend on high friction surfaces as summarized in Table III. These results highlight the importance of considering future rear tire saturation for both low and high values of surface friction.

VI. Conclusion

With only the ability to steer, situations may arise when violation of the stable handling envelope is required to

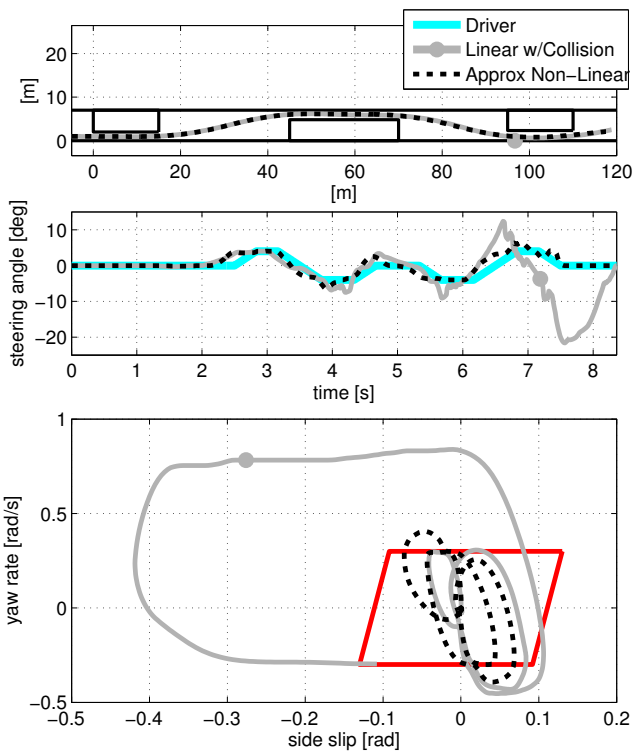

Fig. 8. Double lane change maneuver on low friction surface at 18 [m/s]

TABLE III
MAXIMUM SPEED WITHOUT COLLISION

Surface Friction, μ	Linear Rear Tire Model	Approx. Non-Linear Rear Tire Model
0.90	18 [m/s]	22 [m/s]
0.55	14 [m/s]	19 [m/s]

avoid a collision with the environment. In these situations, use of successive linearizations enables the controller to consider future rear tire saturation to appropriately steer the vehicle safely without additional computational burden. In addition, the prediction of future vehicle states throughout the prediction horizon is improved, giving advanced warning on pending challenges to the combined objectives of vehicle stability and collision avoidance. This advanced warning may allow the controller time to safely reduce the vehicle's speed using brake actuation, in order to ensure that the vehicle's future trajectory will always safely adhere to both safe driving envelopes. Future work focuses on the development of this comprehensive envelope controller that will be capable of ensuring vehicle safety through augmentation of the driver's steer and brake commands.

ACKNOWLEDGMENT

The authors would like to thank the NISSAN MOTOR Co., Ltd. and project team members Susumu Fujita, Yoshitaka Deguchi, and Hikaru Nishira for sponsoring this research. Joseph Funke is supported by a Graduate Research Fellowship from the National Science Foundation.

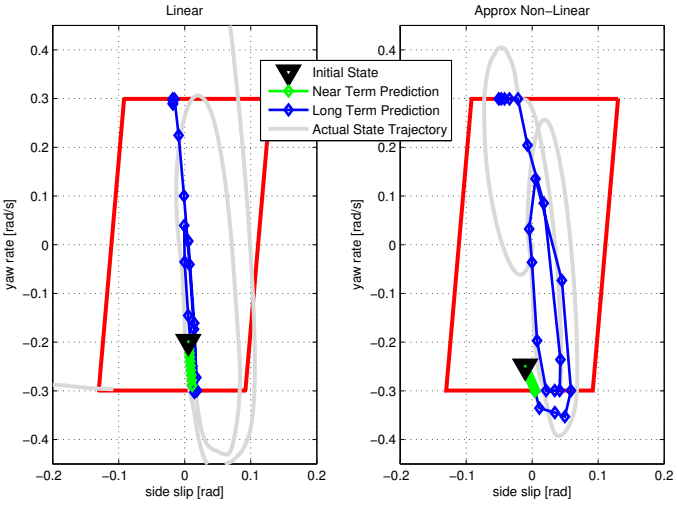

Fig. 9. Comparison of the planned safe trajectory midway through the double lane change manuever on low friction surface at 18 [m/s]

REFERENCES

[1] Y.-H. Hsu, S. Laws, and J. Gerdes, "Estimation of tire slip angle and friction limits using steering torque," *IEEE Transactions on Control Systems Technology*, vol. 18, no. 4, pp. 896–907, July 2010.

[2] T. Kawabe, H. Nishira, and T. Ohtsuka, "An optimal path generator using a receding horizon control scheme for intelligent automobiles," in *IEEE International Conference on Control Applications*, 2004.

[3] P. Falcone, F. Borrelli, E. Tseng, J.Asgari, and D. Hrovat, "Linear time-varying model predictive control and its application to active steering systems: Stability analysis and experimental validation," *International Journal of Robust and Nonlinear Control*, vol. 18, pp. 862–875, 2007.

[4] J. P. Timings and D. J. Cole, "Minimum maneuver time calculation using convex optimization," *Journal of Dynamic Systems Measurements and Control*, vol. 135, March 2013.

[5] S. M. Erlien, S. Fujita, and J. C. Gerdes, "Safe driving eenvelope for shared control of ground vehicles," in *Advances in Automotive Control, 2013 IFAC Symposium*, Sept 2013.

[6] E. Fiala, "Lateral forces on rolling pneumatic tires," in *Zeitschrit V.D.I*, vol. 96, 1954.

[7] H. B. Pacejka, *Tire and Vehicle Dynamics*, 3rd ed. Butterworth-Heinemann, 2012.

[8] C. E. Beal and J. C. Gerdes, "Model predictive control for vehicle stabilization at the limits of handling," *IEEE Transactions on Control Systems Technology*, 2013.

[9] J. Yi, J. Li, J. Lu, and Z. Liu, "On the stability and agility of aggressive vehicle maneuvers: A pendulum-turn maneuver example," *IEEE Transactions on Control Systems Technology*, vol. 20, no. 3, pp. 663–676, May 2012.

[10] J. Mattingley and S. Boyd, "Cvxgen: a code generator for embedded convex optimization," *Optimization and Engineering*, vol. 13, no. 1, pp. 1–27, 2012.

[11] J. Mattingley, Y. Wang, and S. Boyd, "Code generation for receding horizon control," in *2010 IEEE International Symposium on Computer-Aided Control System Design (CACSD)*, sept. 2010, pp. 985 –992.